Hong Kong J Radiol. 2023;26:217-32. Epub 15 Sep 2023 | https://doi.org/10.12809/hkjr2217525

PICTORIAL ESSAY

# Conventional and Advanced Post-treatment Magnetic Resonance Imaging of Primary and Metastatic Brain Tumours: A Pictorial Essay

**JCY Lau[1], AYT Lai[1], KYK Tang[1], CY Chu[1], PY Wu[2], WK Kan[1]**

*[1]Department of Radiology, Pamela Youde Nethersole Eastern Hospital, Hong Kong SAR, China*
*[2]Department of Clinical Oncology, Pamela Youde Nethersole Eastern Hospital, Hong Kong SAR, China*

## INTRODUCTION

Both primary and secondary brain neoplasms are commonly encountered in neuroimaging. Glioblastoma is the most common primary malignant brain tumour in adults.[1] Mortality remains high despite development of different treatment options with combinations of surgery, radiotherapy, and chemotherapy. The 2-year and 5-year survival rates after diagnosis of glioblastoma are reported to be approximately 26.5%[2] and 5% to 10%,[3] respectively. Evaluation of treatment response and detection of treatment-related complications are crucial in patient management and rely heavily on neuroimaging.

Brain tumour treatment response criteria have been established to evaluate treatment progression or regression of gliomas. Currently, the most widely used set of criteria is the Response Assessment in Neuro-Oncology (RANO) criteria.[1] First proposed in 2010, the RANO criteria assess measurable disease, non-measurable disease, use of corticosteroids, and clinical status[2] for assessment of treatment response, which are discussed in this article.

There are significant overlapping features with conventional magnetic resonance imaging (MRI) techniques among treatment response and disease progression and/or treatment-related complications. Advanced MRI techniques, including MR spectroscopy (MRS) and perfusion, are useful adjuncts to facilitate interpretation of post-treatment brain tumour images, especially in identifying pseudoprogression or pseudoresponse.[4,5]

This pictorial essay illustrates the broad spectrum of treatment-related complications, the different treatment responses of brain tumours as classified by the RANO criteria, and utilisation of advanced MRI techniques in identifying treatment-related changes, e.g., pseudoprogression or pseudoresponse.

*Correspondence: Dr JCY Lau, Department of Radiology, Pamela Youde Nethersole Eastern Hospital, Hong Kong SAR, China*
*Email: lcy486@ha.org.hk*

Submitted: 5 Jan 2022; Accepted: 17 May 2022.

Contributors: JCYL and AYTL designed the study. JCYL, AYTL and PYW acquired the data. JCYL and AYTL analysed the data. JCYL drafted the manuscript. All authors critically revised the manuscript for important intellectual content. All authors had full access to the data, contributed to the study, approved the final version for publication, and take responsibility for its accuracy and integrity.

Conflicts of Interest: All authors have disclosed no conflicts of interest.

Funding/Support: This study received no specific grant from any funding agency in the public, commercial, or not-for-profit sectors.

Data Availability: All data generated or analysed during the present study are available from the corresponding author on reasonable request.

Ethics Approval: The study was approved by the Hong Kong East Cluster Research Ethics Committee of Hospital Authority, Hong Kong (Ref No.: HKECREC-2022-001). A waiver for written informed consent of patients was granted by the Committee as this manuscript is for pictorial review only and does not involve patient treatment/procedures.

## TREATMENT RESPONSE ASSESSMENT USING THE RESPONSE ASSESSMENT IN NEURO-ONCOLOGY CRITERIA

### Definitions

Measurable disease is defined as bi-dimensionally (two perpendicular diameters) contrast-enhancing lesions of at least 10 mm, while non-measurable disease is defined as either unidimensionally measurable lesions, masses with unclear margins, or lesions with maximal perpendicular diameters of <10 mm.[4] Cysts or the surgical cavity should be considered non-measurable unless there is a nodular component measuring at least 10 mm in diameter.[4] Lesions with T2/fluid-attenuation inversion recovery (FLAIR) hyperintense signals are considered non-measurable.[1]

### Multiple Lesions

A minimum of two and a maximum of five target lesions may be counted to reflect tumour burden. The sum of the products of the perpendicular diameters are used for determining treatment response. Although the largest lesions are commonly selected, emphasis should be made on lesions with reproducible measurements.[4]

Categories of treatment response, which are from Leao et al[1] and Wen et al,[4] are summarised as follows.

#### *Complete response*

It requires all of the following: complete disappearance of all enhancing measurable and non-measurable diseases sustained for at least 4 weeks; no new lesions; and stable or improved non-enhancing (T2/FLAIR hyperintensity) lesions. Patients must be off corticosteroids (or on physiological replacement doses only) and should be in a stable or clinically improved status (Figure 1).[4]

#### *Partial response*

It requires all of the following: ≥50% decrease in the sum of products of perpendicular diameters of all measurable enhancing lesions compared with baseline scan sustained for at least 4 weeks; no progression of non-measurable disease; no new lesions; stable or improved non-enhancing (T2/FLAIR hyperintensity) lesions on the same or a lower dose of corticosteroids compared with baseline scan; and the patient being on a corticosteroid that is not greater than the dose at time of the baseline scan and should be in stable or clinically improved status (Figure 2).[4]

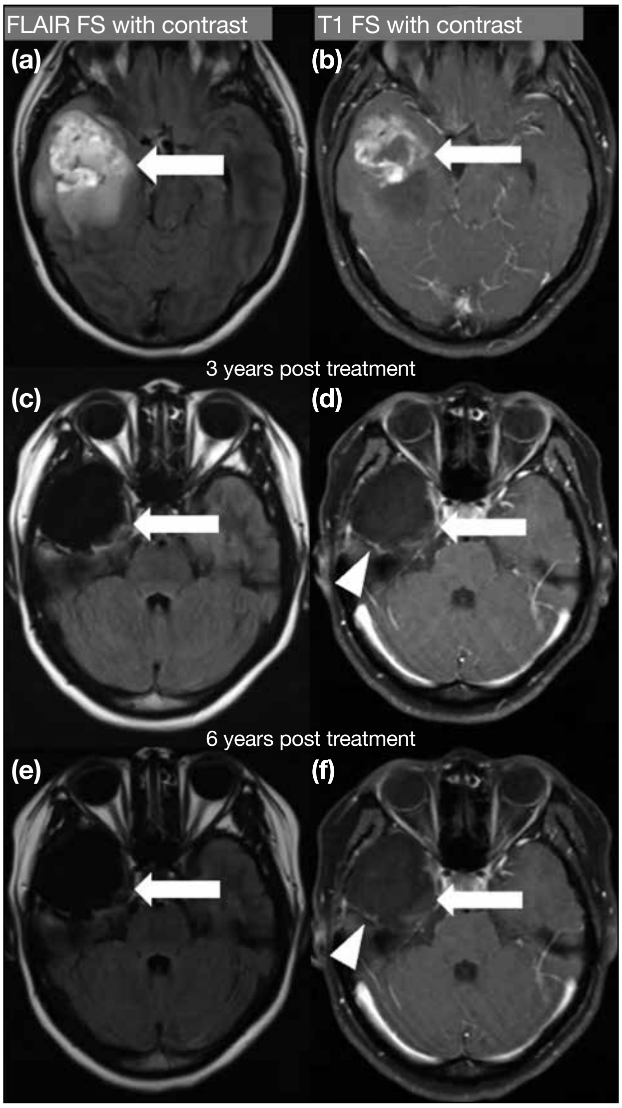


**Figure 1.** Complete response shown in post-contrast fluid-attenuation inversion recovery (FLAIR) fat suppression (FS) sequences (a, c, and e) and post-contrast T1-weighted FS sequences (b, d, and f). An ill-defined contrast-enhancing mass with vasogenic oedema was demonstrated in the right temporal lobe in a 20-year-old patient (arrows in [a] and [b]). Gross total excision was performed, confirming oligodendroglioma. No adjuvant therapy was prescribed. Follow-up magnetic resonance imaging performed 3 years (c and d) and 6 years (e and f) later revealed encephalomalacia (arrows in [c] to [f]) and stable enhancement (arrowheads in [d] and [f]) of the dura, suggesting postoperative changes. Features are compatible with complete response.

#### *Stable disease*

It requires all of the following: not qualified for complete response, partial response or progression; stable non-enhancing (T2/FLAIR hyperintensity) lesion; the patient being on the same or lower dose of corticosteroids compared with baseline scan and should be in clinically stable status (Figures 2 and 3).[1,4]

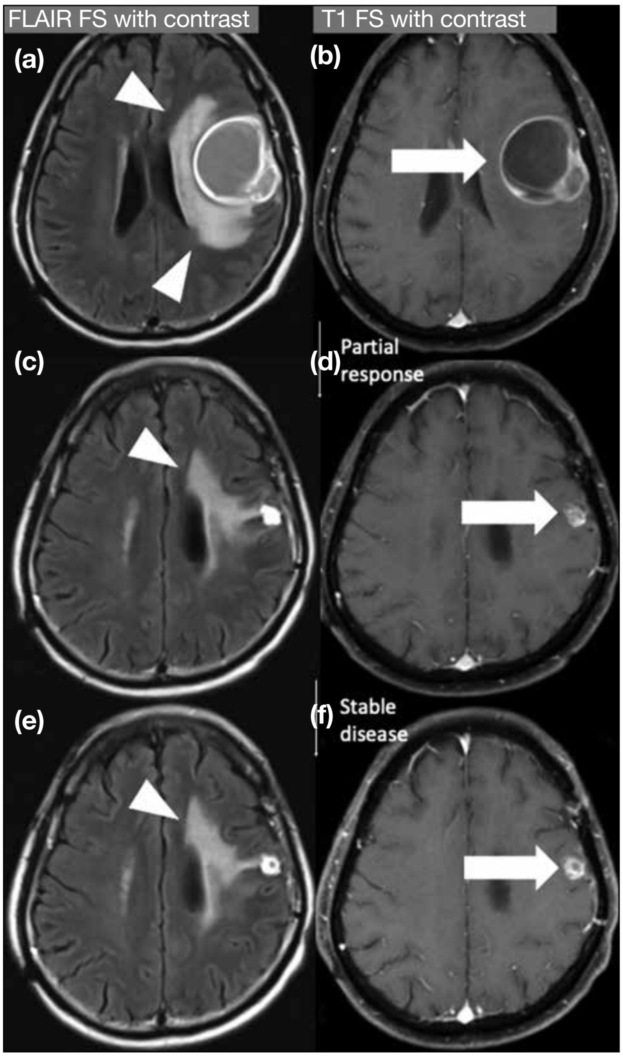


**Figure 2.** Partial response and stable disease shown in post-contrast fluid-attenuation inversion recovery (FLAIR) fat suppression (FS) sequences (a, c, and e) and post-contrast T1-weighted FS sequences (b, d, and f). (a and b) A rim-enhancing complex cystic lesion with eccentric enhancing-solid component (arrow in [b]) and perifocal FLAIR hyperintensity (arrowheads in [a]) are illustrated in the left frontal lobe of a 73-year-old patient. Histology of World Health Organization grade 4 glioblastoma was confirmed with gross total excision. The patient was then managed with adjuvant chemoirradiation. Follow-up magnetic resonance imaging (MRI) at 1 year (c and d) revealed significant reduction in the left frontal contrast-enhancing lesion (arrow in [d]) and perilesional FLAIR hyperintensity (arrowhead in [c]), compatible with partial response. MRI performed 2 years after the excision (e and f) demonstrated no significant change (arrow in [f] and arrowhead in [e]), suggestive of stable disease.

### *Disease progression*

It is defined by any of the following: ≥25% increase in sum of the products of perpendicular diameters of enhancing lesions compared with the smallest tumour measurement obtained either at baseline scan (if no decrease) or best response; on stable or increasing doses of corticosteroids; significant increase in non-enhancing T2/FLAIR hyperintensity lesion on stable or increasing doses of corticosteroids compared with baseline scan or best response after initiation of therapy, not caused by comorbid events; any new lesion; clear clinical deterioration not attributable to other causes apart from the tumour or changes in corticosteroid dose; failure to return for evaluation as a result of death or deteriorating condition; or clear progression of non-measurable disease (Figures 4 to 6).[1,4]

## PSEUDOPROGRESSION

The Stupp protocol, consisting of maximal safe excision and adjuvant radiotherapy with concurrent and adjuvant temozolomide, is considered the standard of care for glioblastoma.[2]

New or progressive contrast enhancement can develop as a result of irradiation or treatment, in addition to true tumour progression. The RANO criteria define phenomenon that eventually subsides without alteration of management as pseudoprogression (Figures 7 and 8),[1,4] with reported incidence of up to 21% to 36%.[1,6] It is more commonly encountered in glioblastoma with positive methylated $O^6$-methylguanine–DNA methyltransferase gene promoter, which carries a better prognosis.

Pseudoprogression is likely the consequence of transient increase in tumour vasculature and permeability due to irradiation and is exacerbated by temozolomide. During the early post-radiotherapy period (usually around 3-6 months), most new lesions on MRI represent a mixture of residual tumour and pseudoprogression. The predominant component will dictate the clinical and radiological picture over time. Imaging features during this period might be difficult to interpret even with the help of advanced MRI techniques. The RANO criteria suggest that progression can only be determined <12 weeks after completion of adjuvant chemoradiation if the new enhancing focus is outside of the high-dose radiation field or by unequivocal histological findings.[4] Classically, pseudoprogression presents with a mass of 'Swiss cheese' appearance[1] (Figure 7) on conventional imaging. At 3 to 6 months after the commencement of chemoradiation, when there are new or progressive lesions, advanced MRI might potentially aid radiologists in interpreting these lesions.

### Magnetic Resonance Perfusion

Dynamic susceptibility contrast (DSC) and dynamic contrast enhancement (DCE) are the most commonly

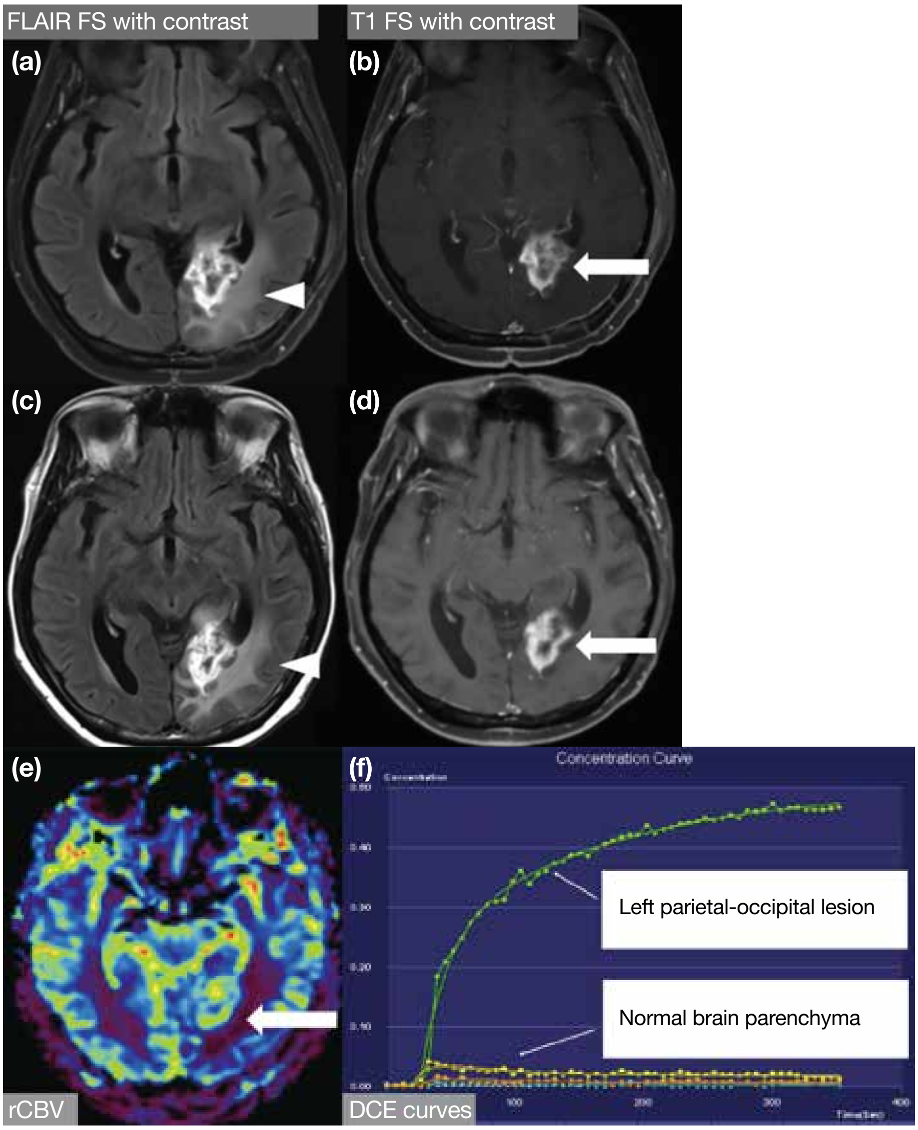


**Figure 3.** Stable disease shown in post-contrast fluid-attenuation inversion recovery (FLAIR) fat suppression (FS) sequences (a and c) and post-contrast T1-weighted FS sequences (b and d). (e) shows the relative cerebral blood volume (rCBV) colour map while (f) shows the dynamic contrast enhancement (DCE) concentration-time curve. A 53-year-old patient underwent subtotal excision of a left parietooccipital tumour, confirming a glioblastoma with negative *O*[6]-methylguanine–DNA methyltransferase methylation and isocitrate dehydrogenase wild-type. The patient was then managed with combined radiotherapy and temozolomide. Follow-up magnetic resonance imaging (MRI) performed 5 months (a and b) and 9 months (c and d) after chemoradiotherapy demonstrated no significant interval change in the left parietal-occipital contrast-enhancing lesion (arrows in [b] and [d]) and the perilesional FLAIR hyperintense signals (arrowheads in [a] and [c]). MR perfusion (e and f) performed 9 months after chemoradiotherapy illustrated increase in rCBV (arrow in [e]), rapid initial uprise of the concentration-time curve and larger initial area under the curve at the left parietal-occipital lesion, suggestive of residual tumour. Features are in keeping with stable disease.

used perfusion techniques for assessment of tumour perfusion. DSC perfusion imaging utilises the susceptibility gradient from loss of T2* signal secondary to the passage of contrast through brain tissue and hence derives the relative cerebral blood volume (rCBV).[1,6] High rCBV would suggest the presence of tumour (Figures 5 and 6) due to their hypervascularity, whereas low rCBV may represent post-treatment changes (Figure 8).[5]

DCE perfusion involves plotting a contrast signal–time curve, also known as a concentration-time curve, enhancement-time curve or permeability curve, by estimating the extravasation of contrast from the intravascular space into the extravascular extracellular space (EES).[7] Measurements derived from this permeability curve have been found to provide valuable clinical information concerning tumour behaviour. Quantification of enhancement characteristics can be performed using a range of techniques, from simple measures of the rate of enhancement to complex algorithmic analyses that apply pharmacokinetic models to the imaging data, one of which bears the intention of measuring the transfer constant of contrast between the plasma and the EES, i.e., the time-dependent leakage constant $K^{trans}$.[7] $K^{trans}$ is dependent on plasma blood flow, vascular permeability, and capillary surface area. The slope of the concentration-time curve is therefore one of the factors in determining the level of this constant.[8] $K^{trans}$ is described to be elevated, compared to that of normal brain tissue, in tumour progression (Figures 5 and 6) and reduced in pseudoprogression (Figure 8).[1,4,6] However,

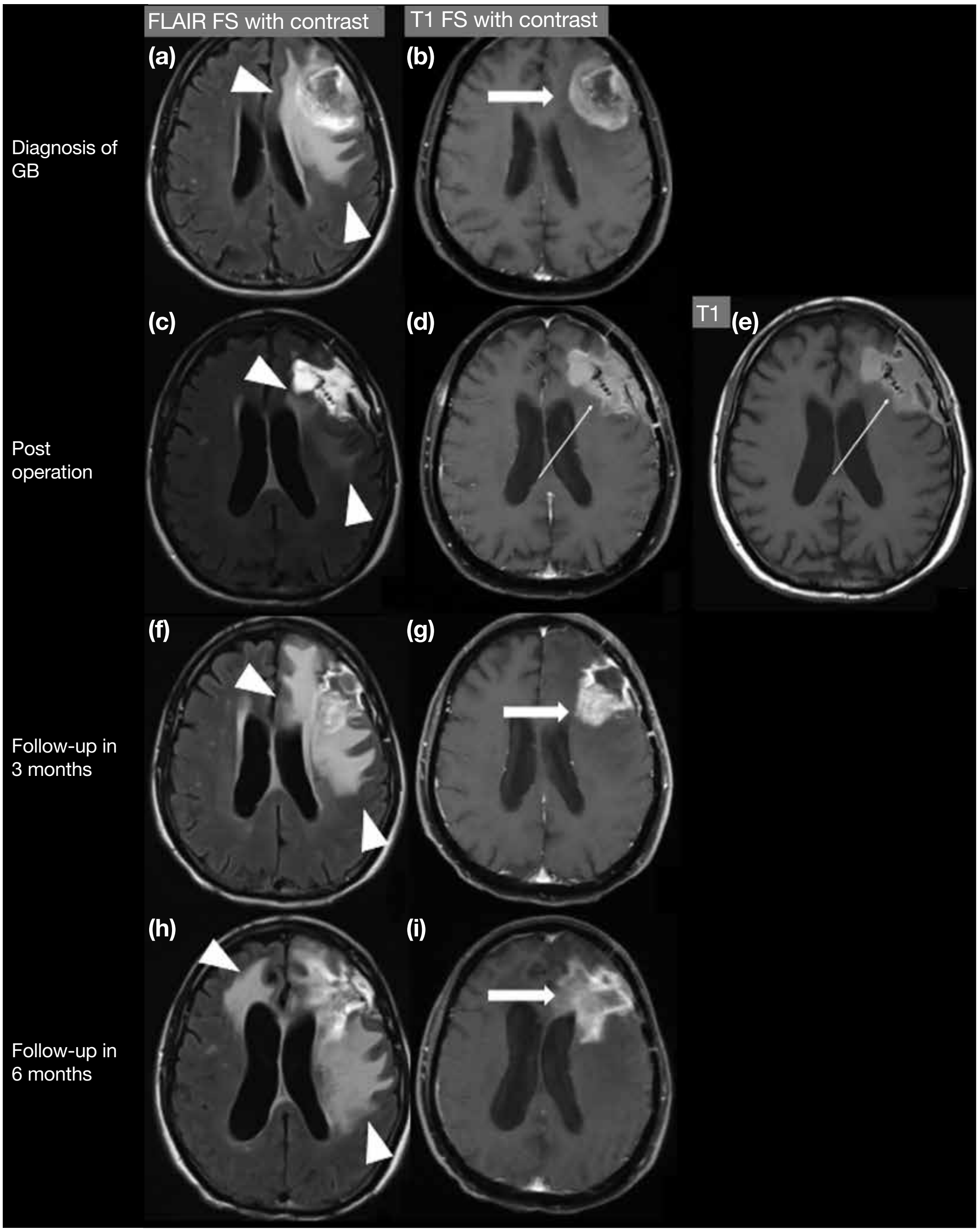


**Figure 4.** Disease progression shown in post-contrast fluid-attenuation inversion recovery (FLAIR) fat suppression (FS) sequences (a, c, f, and h), post-contrast T1-weighted FS sequences (b, d, g, and i), and T1-weighted sequence (e). A 72-year-old patient presented with a heterogeneously enhancing left frontal mass (arrow in [b]) with perilesional FLAIR hyperintense signals (arrowheads in [a]). The patient underwent gross total excision of the tumour with pathology suggesting glioblastoma (GB). Early postoperative magnetic resonance imaging (MRI) [c, d, and e] showed significant reduction in size of the left frontal tumour and FLAIR signals (arrowheads in [c]) with presence of T1-weighted hyperintensity (thin arrows in [d] and [e]), suggesting subacute blood products. Radiotherapy was prescribed and follow-up MRI performed 3 months later (f and g) revealed increased contrast enhancement (arrow in [g]) and FLAIR hyperintensity (arrowheads in [f]) in the left frontal-parietal region. Combined with the findings in Figure 5, features are most compatible with disease progression, which was confirmed in subsequent follow-up MRI (h and i), showing increase in size of the enhancing mass (arrow in [i]) and perilesional FLAIR hyperintensity (arrowheads in [h]).

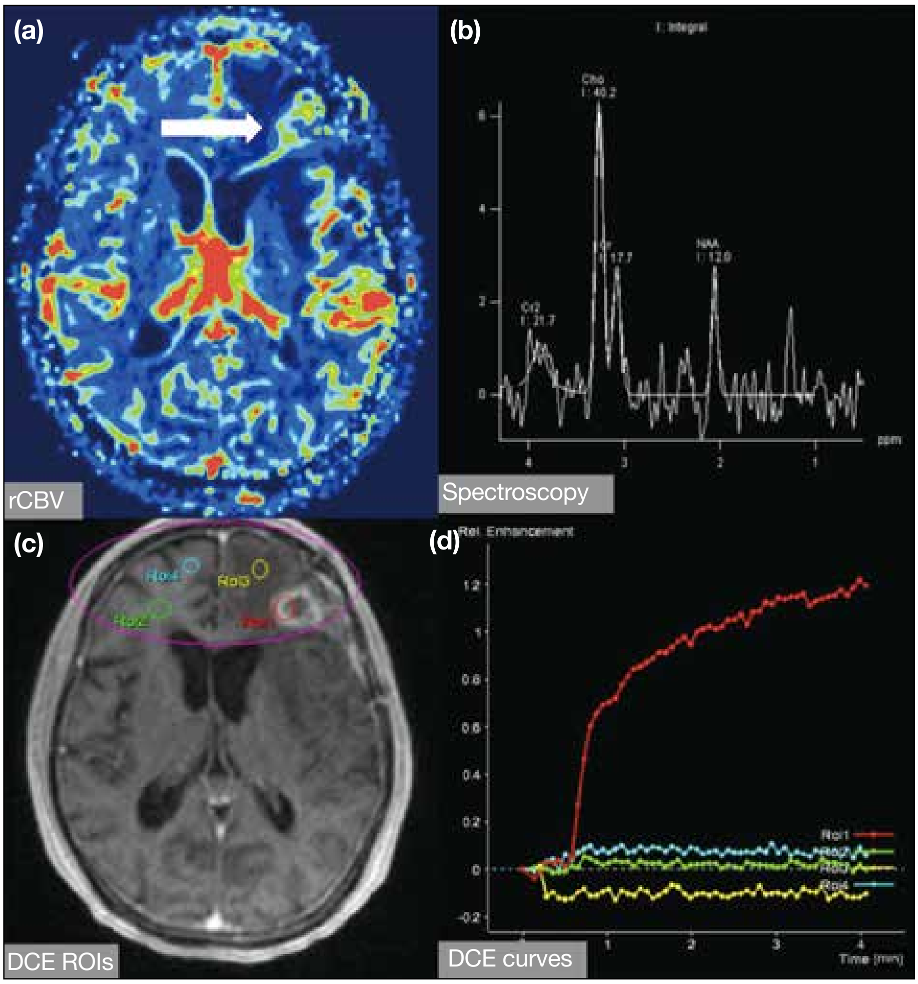


**Figure 5.** Disease progression in the same patient as in Figure 4 with magnetic resonance (MR) perfusion and MR spectroscopy (MRS) performed 3 months after excision of the left frontal glioblastoma. (a) shows relative cerebral blood volume (rCBV) map, (b) shows MRS, (c) shows dynamic contrast enhancement (DCE) regions of interest [ROIs], and (d) shows DCE concentration-time curves. The left frontal lesion demonstrated elevated rCBV (arrow in [a]), an elevated choline (Cho) peak with reversed Cho-to-*N*-acetylaspartate (NAA) ratio (b), a rapid rise in initial DCE enhancement, and a larger initial area under the curve as compared to the normal brain parenchyma (d). Together with the findings in Figure 4, features are in keeping with disease progression.

detailed discussion on the compartmental models is beyond the scope of this article.

The concentration-time curve derived from the DCE perfusion consists of two phases, namely the initial vascular phase and the subsequent delayed equilibrium phase.[9] The initial upslope reflects early enhancement, mostly from the contrast agent in the blood vessels and early leakage into the EES due to disrupted blood-brain barrier, which is again dependent on blood flow and vascular surface area. On the other hand, the delayed equilibrium phase includes mostly delayed permeability and slow accumulation of contrast agent into the EES, depending on the backflow of contrast agent into the intravascular compartment. These factors are affected by the volume of EES, interstitial pressure, and total vascular area.

Compared to treatment-induced necrosis, recurrent or progressive brain tumour shows an elevated maximum slope in the initial vascular phase due to increased blood flow from neo-angiogenesis.[9] The slope of the delayed equilibrium phase is higher in treatment-induced necrosis as a result of low cellularity and more tissue damage, allowing more retention of contrast in the EES and less backflow to the intravascular compartment, resulting in reduced washout.[9]

The area under the curve (AUC) of the concentration-time curve can also help differentiate between recurrent tumour and radiation necrosis. The initial AUC (iAUC) is found to be higher in recurrent tumour than in radiation necrosis, as a result of neovascularity in the tumour.[9] The ratio of iAUC to final AUC (defined as between 320 and 350 seconds after contrast agent arrival in the same enhancing voxel of interest as iAUC) is found to be elevated in recurrent tumours compared to radiation necrosis, explained by the fact that high vascularity in recurrent tumour results in elevated iAUC while more retention of contrast in the EES due to low cellularity and more tissue damage in radiation necrosis contributes to higher final AUC.[10]

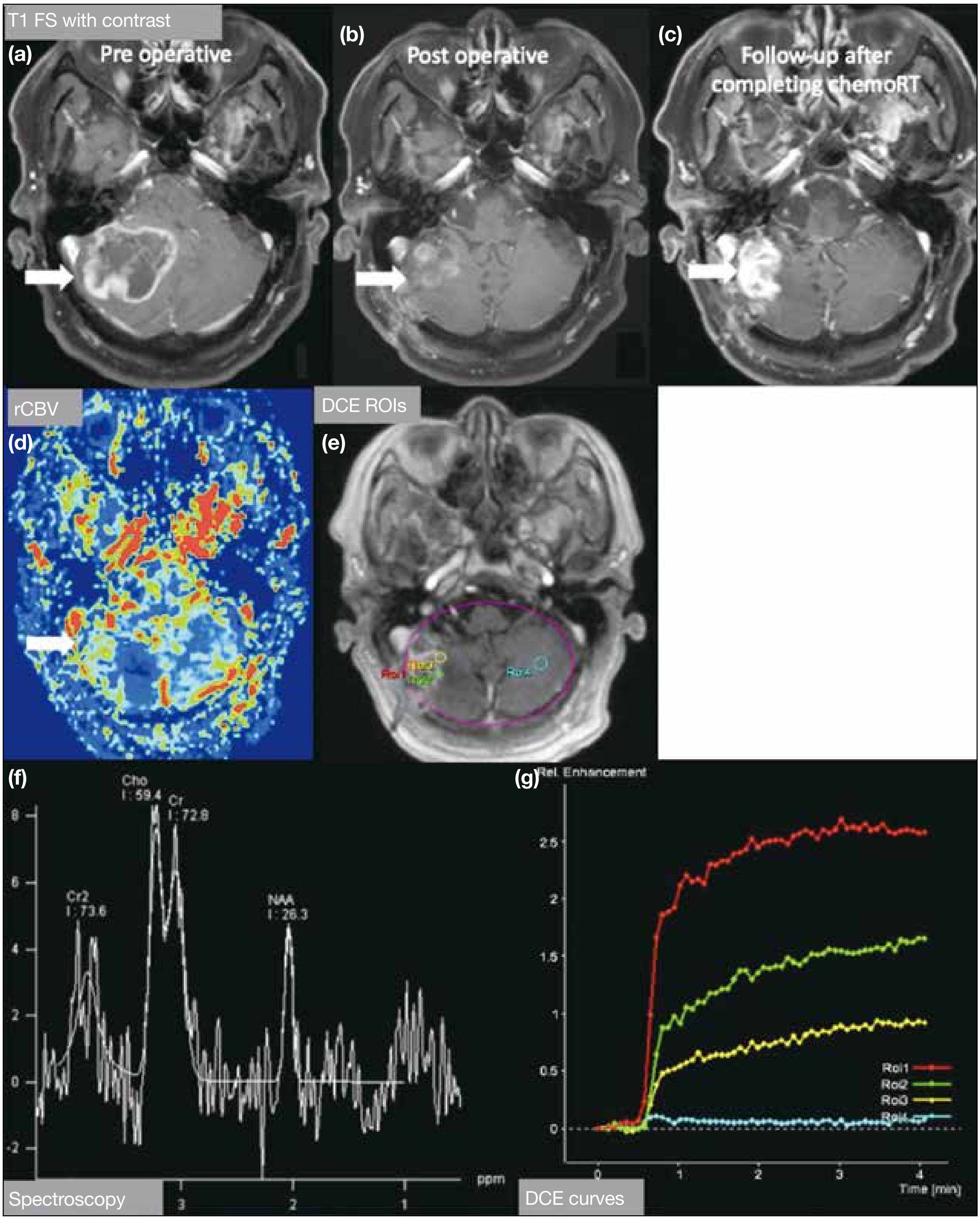


**Figure 6.** Disease progression. A 79-year-old patient with right cerebellar glioblastoma underwent gross total excision and managed with adjuvant radical radiotherapy (a to c). The images show a contrast enhancing lesion at right cerebellum on post-contrast T1-weighted fat saturation (FS) sequences at preoperation (arrow in [a]), 1 month postoperation (arrow in [b]), and after completing chemoradiotherapy (arrow in [c]); (d) shows relative cerebral blood volume (rCBV) colour map while (f) shows magnetic resonance spectroscopy. After completing chemoradiotherapy, the enlarging right cerebellar mass (arrow in [c]) showed elevated cerebral perfusion (arrow in [d]) and an elevated choline (Cho) peak with a reversed Cho-to–*N*-acetylaspartate (NAA) ratio of >2 (f). Dynamic contrast enhancement (DCE) regions of interest (ROIs) were demonstrated in (e) [purple circle]. Steep upslope of the concentration-time curves and larger initial areas under the curve were illustrated as compared to the normal left cerebellar hemisphere (g). This was histologically proven to be tumour recurrence and disease progression.

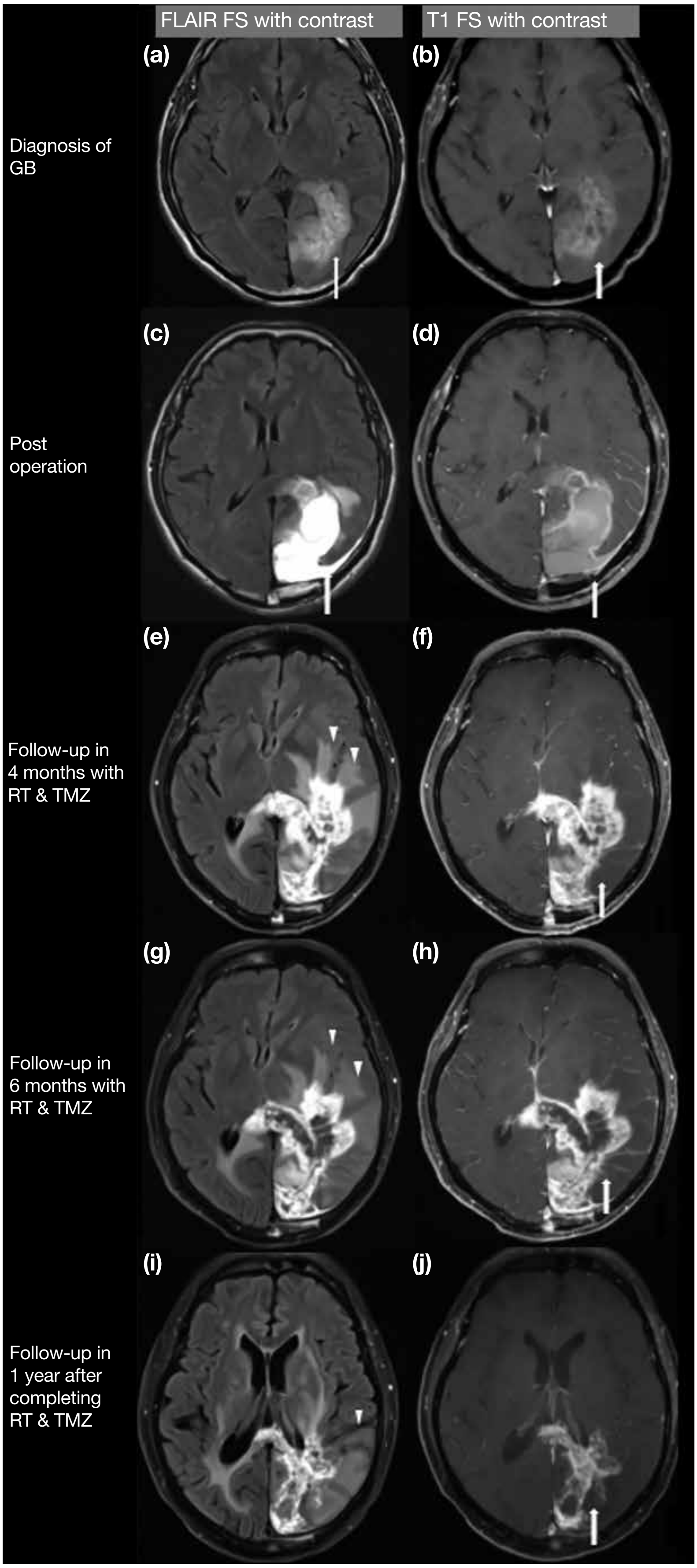


**Figure 7.** Pseudoprogression shown in post-contrast fluid-attenuation inversion recovery (FLAIR) fat suppression (FS) sequences (a, c, e, g, and i) and post-contrast T1-weighted images with FS sequences (b, d, f, h, and j). A 63-year-old patient with an ill-defined enhancing left parietooccipital tumour that was compatible with glioblastoma [GB] (arrows in [a] and [b]) was subsequently removed by near-total excision. Histology showed glioblastoma with positive $O^6$-methylguanine–DNA methyltransferase methylation. Postoperative magnetic resonance imaging (MRI) illustrated no gross parenchymal enhancement (arrows in [c] and [d]). The patient was managed with combined radiotherapy (RT) and temozolomide (TMZ). Follow-up MRI performed 4 months (e and f) and 6 months (g and h) after surgery showed progression of the contrast enhancement with a 'Swiss cheese' appearance (arrows in [f] and [h]) and perilesional FLAIR hyperintense signals (arrowheads in [e] and [g]). Advanced MRI was then performed in view of suspicion of pseudoprogression (see Figure 8). The patient was continued on the same chemotherapy. Follow-up MRI performed 1 year after completion of the adjuvant therapy (i and j) demonstrated decreased enhancement and FLAIR hyperintensities (arrowhead in [i] and arrow in [j]). The constellation of the findings was compatible with pseudoprogression.

 Hong Kong J Radiol. 2023;26:217-32

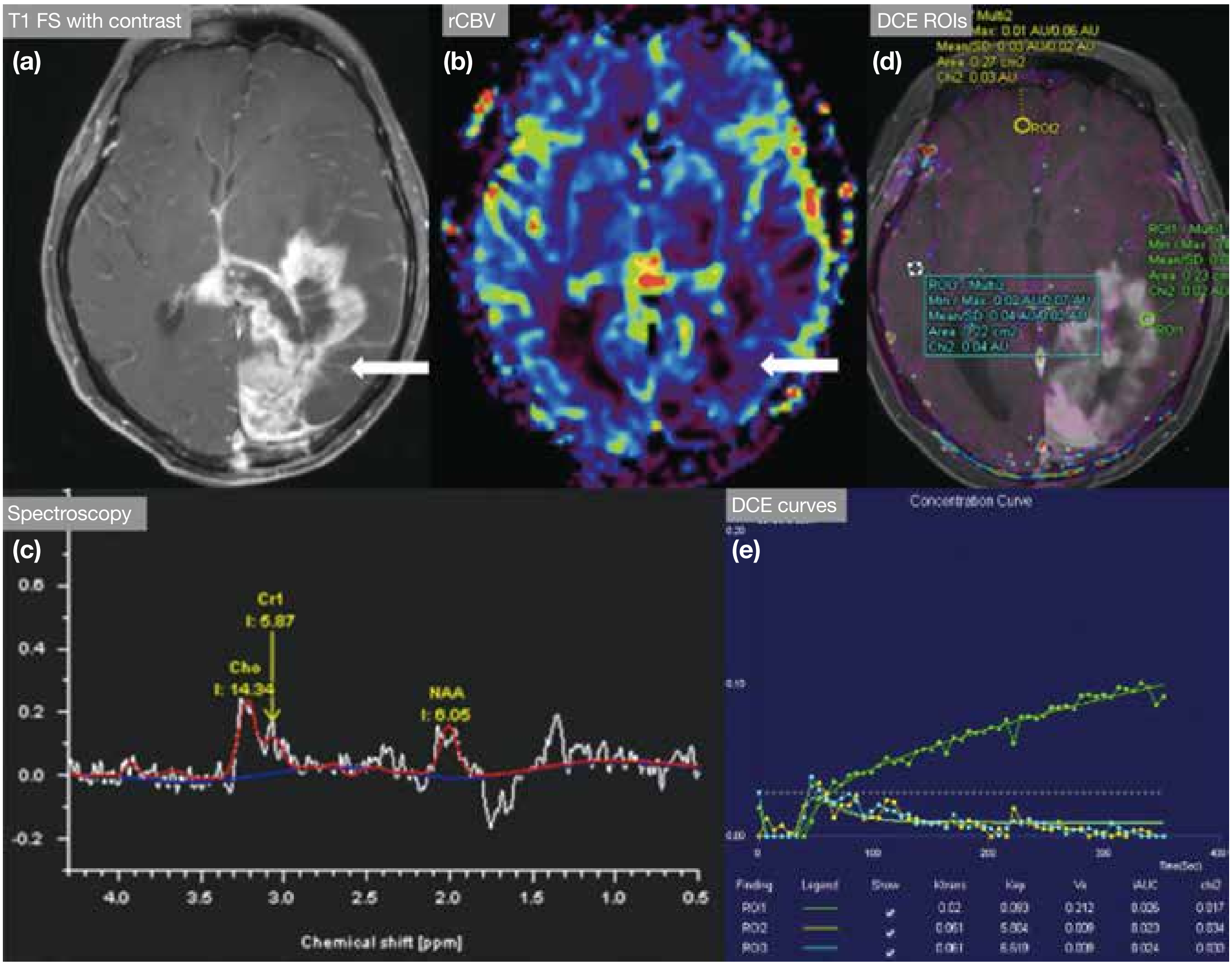


**Figure 8.** Pseudoprogression in the same patient as in Figure 7 at 6 months after commencement of radiotherapy and temozolomide. Post-contrast T1-weighted fat saturation (FS) sequence (a), relative cerebral blood volume (rCBV) colour map (b), magnetic resonance spectroscopy [MRS] (c), dynamic contrast enhancement (DCE) regions of interest (ROIs) [d], and ROI curves (e) reveal a left parietal-occipital contrast enhancing mass (arrow in [a]). Decreased cerebral perfusion was shown (arrow in [b]). The low concentration of metabolites was demonstrated on MRS, suggesting background noise and representing 'empty space'. No significant elevation of the time-dependent leakage constant $K^{trans}$ or initial area under the curve and no rapid uprise of the slope of the concentration-time curve were demonstrated. Features are consistent with pseudoprogression.

Non-contrast MR perfusion techniques, including arterial spin-labelling, can serve as an alternative to DCE and DSC.[1,6] They measure cerebral blood flow by labelling arterial water as the tracer and might be performed in patients in whom gadolinium-based contrast is contraindicated.

These techniques appear promising, but currently there is no established cut-off value that can reliably differentiate between tumour progression and treatment response.

### Magnetic Resonance Spectroscopy

MRS reflects the concentration of brain metabolites based on their precession frequency; representative metabolites include *N*-acetylaspartate (NAA, marker of neuronal viability) and choline (Cho, marker of cell proliferation). Viable tumours typically demonstrate an elevated Cho peak and reduced NAA level[1] (Figures 5 and 6), while treatment-related injury classically reveals decreased Cho and NAA peaks, respectively, and an elevated lipid/lactate peak (Figure 8).[6] Lack of external validation and technical difficulty in evaluating peripheral brain lesions may limit its potential benefits on post-treatment brain tumour imaging interpretation.

## PSEUDORESPONSE

Antiangiogenic agents, such as bevacizumab, antagonise the vascular endothelial growth factor

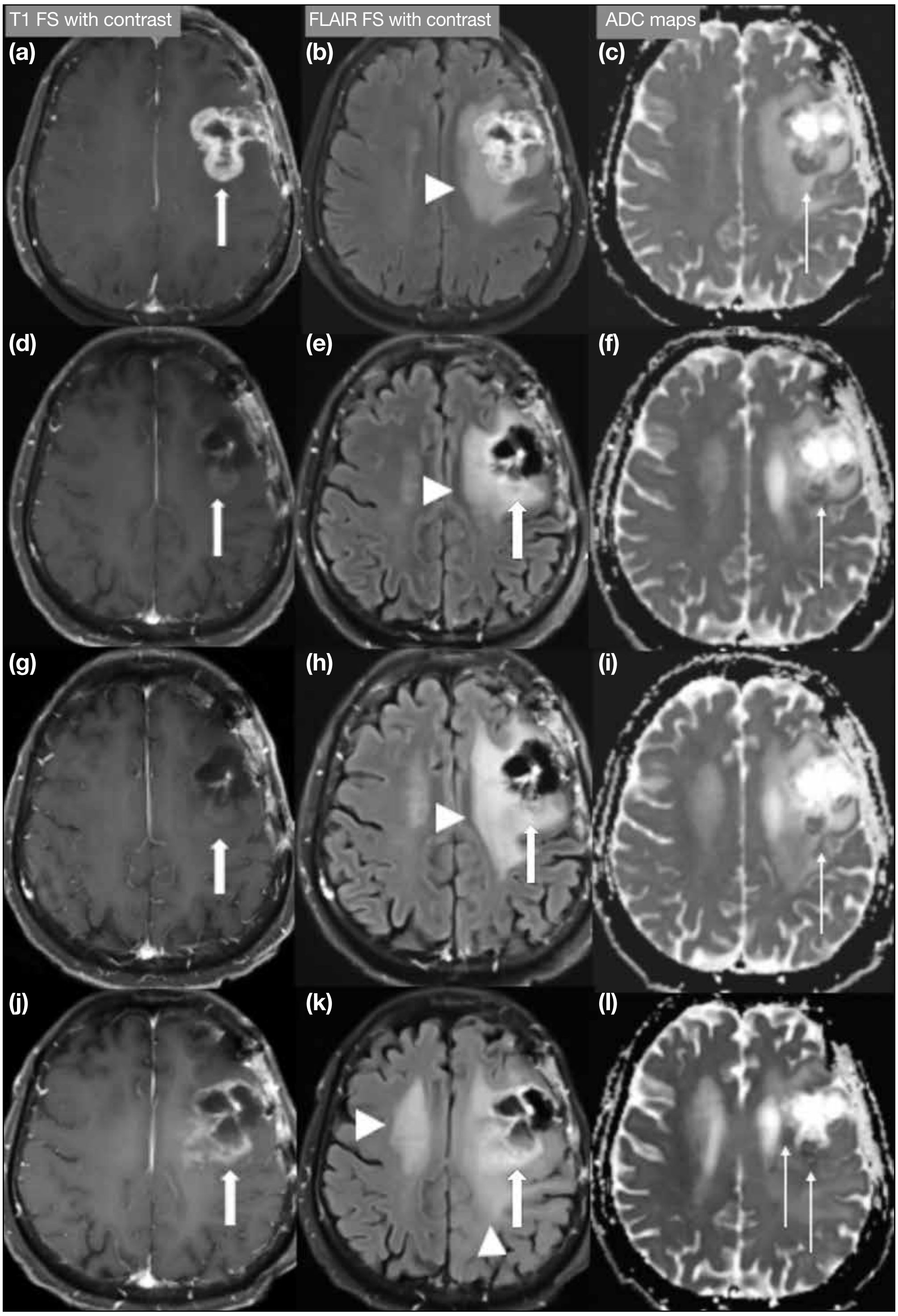


**Figure 9.** Pseudoresponse shown in post-contrast T1-weighted fat suppression (FS) sequence images (a, d, g, and j), post-contrast fluid-attenuation inversion recovery (FLAIR) FS sequence images (b, e, h, and k), and apparent diffusion coefficient (ADC) map images (c, f, i, and l). Disease progression was identified in a 66-year-old patient with a histology-proven left frontal glioblastoma managed with chemotherapy, presenting with a left frontal contrast-enhancing lesion (arrow in [a]) with perilesional FLAIR hyperintensity (arrowhead in [b]) and low ADC value (thin arrow in [c]). Second-line treatment with bevacizumab was started and follow-up magnetic resonance imaging (MRI) performed 4 months later (d to f) showed reduction in contrast enhancement (arrows in [d] and [e]). There was no significant interval change in the perilesional FLAIR hyperintensities (arrowhead in [e]) and low ADC value (thin arrow in [f]) at the left frontal lesion was observed. MRI performed 9 months from commencement of bevacizumab (g to i) demonstrated further reduction in contrast enhancement (arrows in [g] and [h]). Further increase in FLAIR hyperintensities (arrowhead in [h]) and persistent low ADC value (thin arrow in [i]) were illustrated. The treatment regime was continued and disease progression was found in subsequent follow-up MRI (j to l) with increase in contrast enhancement (arrows in [j] and [k]), FLAIR hyperintense signals (arrowheads in [k]), and a new focus of low ADC signal (thin arrows in [l]). The findings are suggestive of pseudoresponse.

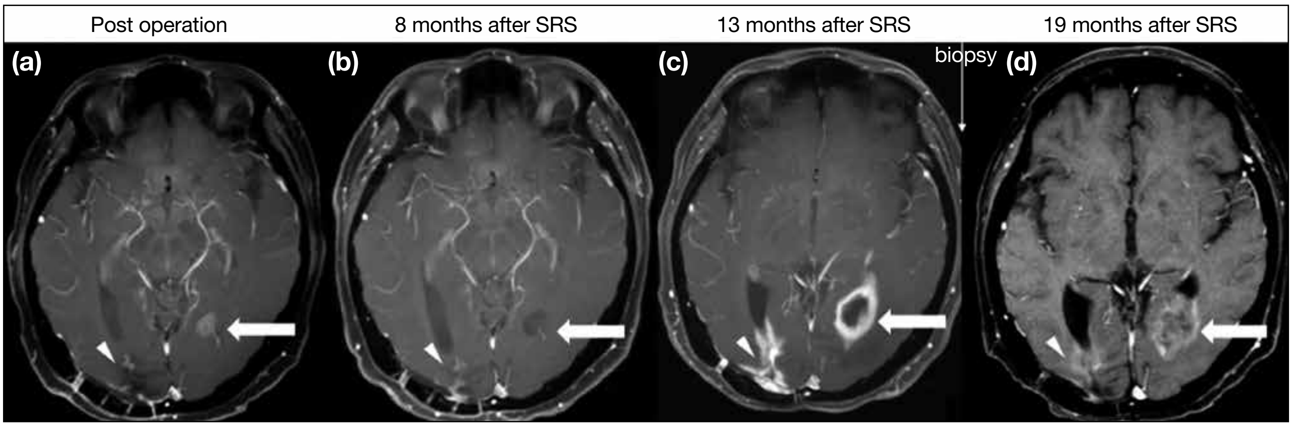


**Figure 10.** Radiation necrosis shown in post-contrast T1-weighted fat saturation sequences. Histologically proven radionecrosis of a left periventricular contrast-enhancing lesion (arrows) is found in a 57-year-old patient with known metastatic breast cancer. Surgical excision of the right periventricular lesion (arrowheads) was performed, with histology confirming metastasis, followed by chemotherapy and stereotactic radiosurgery (SRS) to the surgical bed and the left posterior parietal lesion (a). T1-weighted magnetic resonance imaging (MRI) 8 months after SRS demonstrated reduction in contrast enhancement in the left periventricular lesion and slight increase in contrast enhancement at the right-sided lesion (b). Follow-up MRI performed 5 months later revealed progression in enhancement of both lesions with a cut-pepper–like appearance on the left side. Biopsy of the left-sided lesion suggested radionecrosis (c). Contrast enhancement in both occipital lobes decreased on MRI performed at 6 months' follow-up after the biopsy (d). Histological findings were consistent with radiation necrosis.

receptors to produce an antitumour effect. It is considered a second-line treatment if patients fail the Stupp protocol. It can result in rapid and promising reduction in contrast enhancement but has less effect on non-enhancing infiltrative disease on neuroimaging.[1,4] This discrepancy is characteristic of pseudoresponse (Figure 9). Clinical symptoms and signs may improve after the antiangiogenic agents, but survival benefit remains controversial.[4]

## RADIATION NECROSIS

Radiation necrosis, as the name implies, refers to a delayed necrotic injury of either tumour or normal brain parenchyma, secondary to high radiation exposure as in radiosurgery or high-dose radiotherapy. Most radiation necrosis occurs within a few years after the irradiation.[11] A combination of fibrinoid changes in blood vessels, coagulative necrosis, demyelination, and gliosis can be found on histology. Concomitant use of chemotherapy, targeted therapy for brain metastasis, or immunotherapy may increase the risk of treatment-related necrosis.[11] The typical imaging appearance includes new enhancement at the resection margin that was irradiated at a higher dosage (Figure 10), new periventricular enhancement that lies within the high-dose radiation field, and new distant enhancement within the radiation field but not at the expected sites of tumour spread.[8] On conventional imaging, these can present as a soap-bubble or cut-pepper–like lesion (Figure 10).

On advanced MRI, radiation necrosis can demonstrate reduced rCBV and low permeability on perfusion imaging. Low NAA and Cho peaks and an elevated lipid/lactate peak are classical features observed on MRS (Figure 11).[12]

## STROKE-LIKE MIGRAINE ATTACKS AFTER RADIATION THERAPY SYNDROME

Stroke-like migraine attacks after radiation therapy (SMART) syndrome is a rare, recurrent, and late complication of irradiation with partial to complete recovery.[13] It is more commonly seen in men and clinical presentation includes migraine-like headache, stroke-like focal neurological deficit, and seizures. The pathophysiology is not well understood but proposed mechanisms include cerebral hyperexcitability with impaired autoregulation and endothelial damage as well as reversible radiation-induced vasculopathy. No pathological correlation has been identified on brain biopsy so far and no consensus on effective treatment has been established although antiepileptics and steroids have been used in some of the reported cases of SMART syndrome.[13]

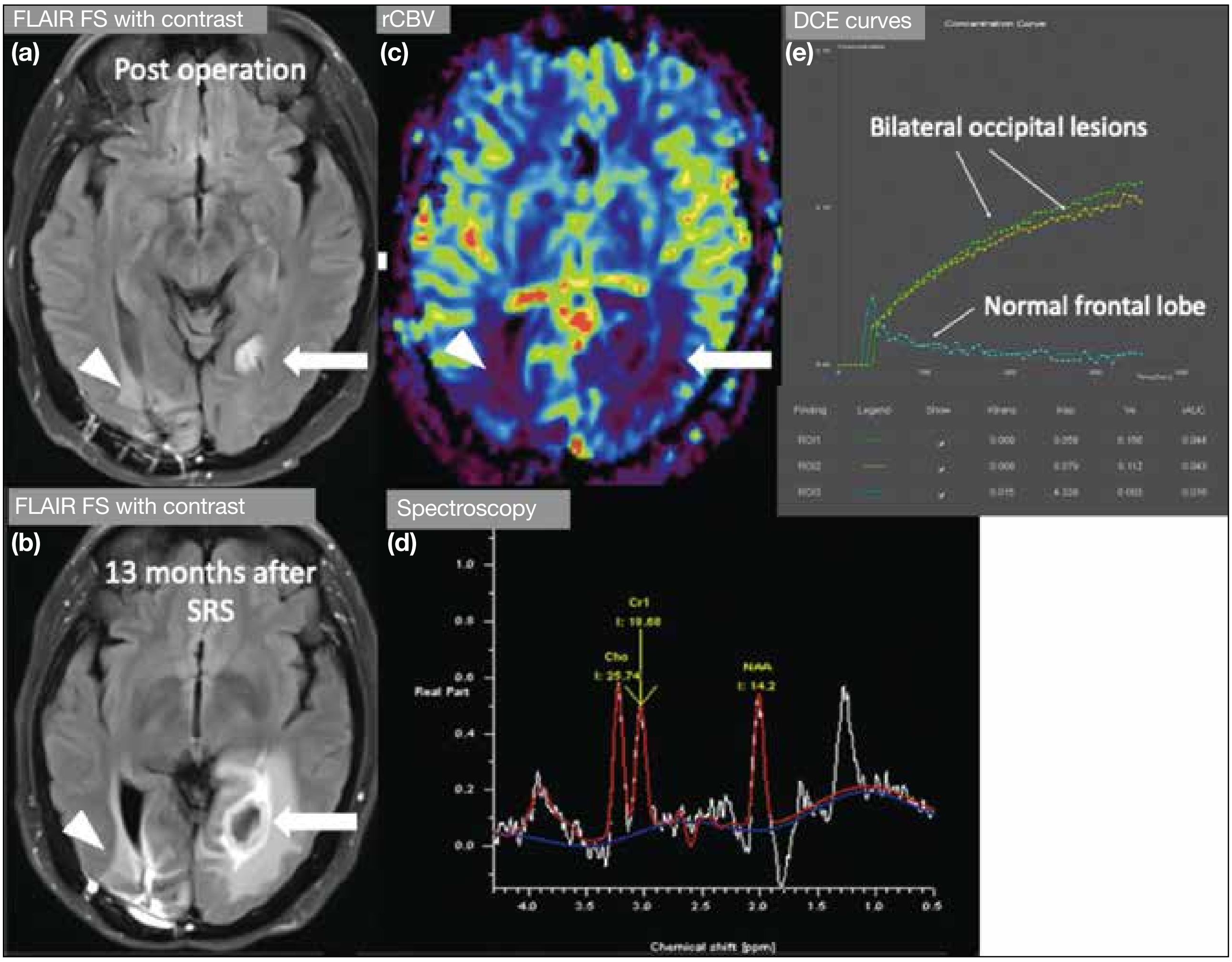


**Figure 11.** Radiation necrosis in the same patient as in Figure 10 with known metastatic breast cancer and bilateral periventricular cerebral lesions. The left periventricular cerebral lesion was histologically proven to be radionecrosis after chemotherapy and stereotactic radiosurgery (SRS). (a) and (b) show post-contrast fluid-attenuation inversion recovery (FLAIR) fat saturation (FS) sequences postoperation and 13 months after SRS, respectively, while (c) shows relative cerebral blood volume (rCBV) colour map, (d) shows magnetic resonance spectroscopy [MRS], and (e) shows dynamic contrast enhancement (DCE) curves in the set of magnetic resonance images performed 13 months after SRS. Increase in perilesional vasogenic oedema was found around both lesions 13 months after SRS (arrow and arrowhead in [b]), as compared to that before SRS (arrow and arrowhead in [a]). Absence of elevated cerebral perfusion was demonstrated (arrow and arrowhead in [c]). On MRS, the concentration of metabolites was found to be reduced, suggesting background noise in the vicinity of 'empty space'. In (e), DCE regions of interest (ROIs) 1 and 2 drawn on bilateral occipital lesions and ROI 3 drawn on normal frontal lobe brain parenchyma revealed no significant increase in the time-dependent leakage constant $K^{trans}$ and mildly increased the initial area under the curve as compared to the normal frontal lobe. In combination with Figure 10, the overall features were compatible with the biopsy-proven radiation necrosis.

Classical imaging findings of SMART syndrome include unilateral cortical gyriform swelling as well as cortical and dural enhancement with or without diffusion restriction, typically found in the parietal-temporal-occipital lobes[13] (Figures 12 and 13). The differential diagnosis of the combined clinical and radiological features includes tumour recurrence/leptomeningeal carcinomatosis, meningoencephalitis, and posterior reversible encephalopathy syndrome (PRES).

Similar to SMART syndrome, PRES commonly manifests as a reversible entity without designated treatment.[14] The pathophysiology of PRES is postulated to be cerebral hyperperfusion from insufficient autoregulation secondary to rapidly developing hypertension and activation of cytokines and inflammatory responses due to systemic disorders such as autoimmune disorders, cytotoxic drugs or sepsis.[5] The typical imaging features of PRES include vasogenic oedema in the bilateral parietal-occipital subcortical white matter, while contrast enhancement and restricted diffusion may be present in up to 20% to 30% of patients,[15]

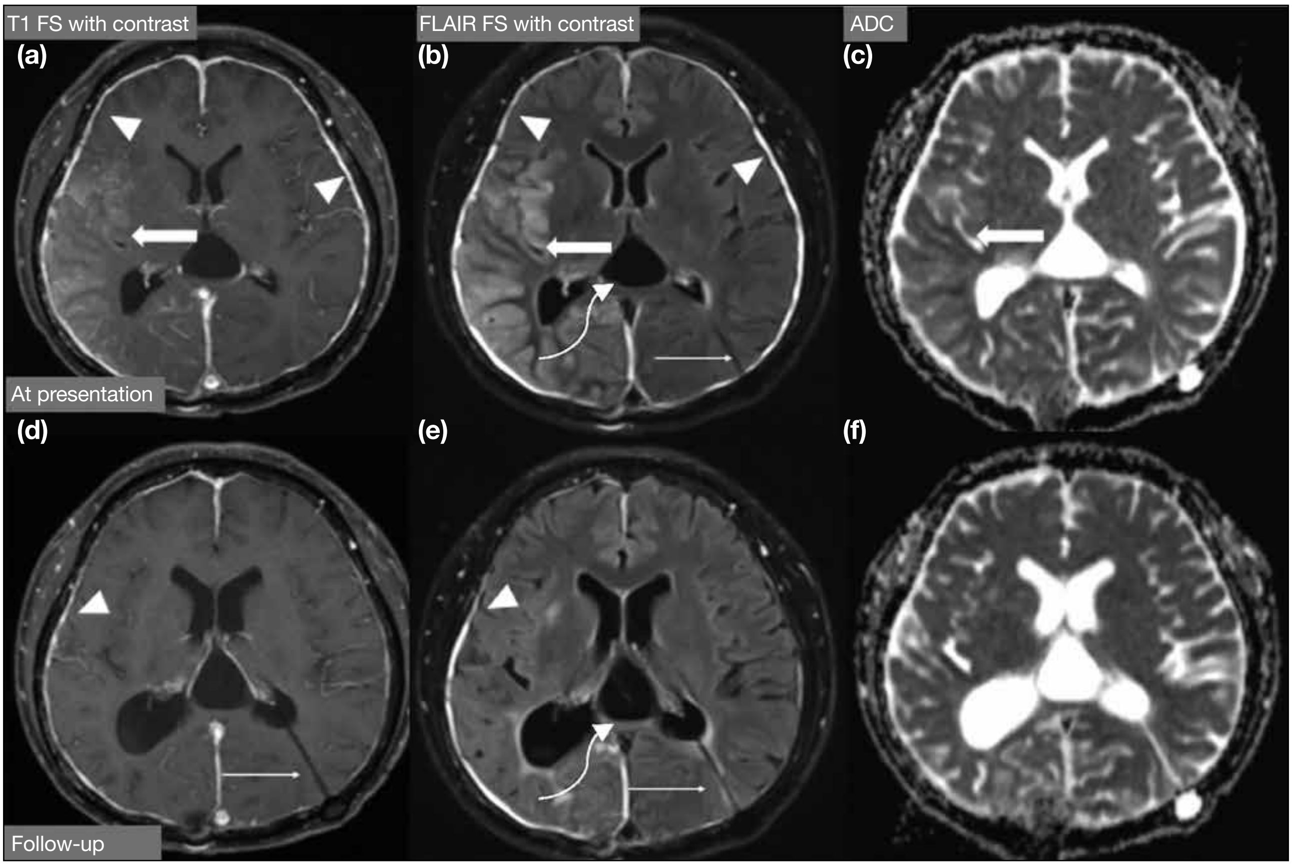


**Figure 12.** Stroke-like migraine attacks after radiation therapy (SMART) syndrome. A 40-year-old patient with history of treated right parietal glioblastoma and stable disease for >5 years presented with headache, seizure, and left hemiplegia. MRI with a post-contrast T1-weighted fat suppression (FS) sequence (a), post-contrast fluid-attenuation inversion recovery (FLAIR) FS sequence (b), and apparent diffusion coefficient (ADC) imaging (c) demonstrated gyriform contrast enhancement and gyral oedema in the right frontal-parietal-occipital cortex with low ADC values (arrows). Incidental note was made of shunt-related diffuse bilateral pachymeningeal enhancement (arrowheads in [a] and [b]) with a left ventriculoperitoneal shunt in situ (thin arrows in [b], [d], and [e]). Follow-up post-contrast T1-weighted FS sequence (d), post-contrast FLAIR FS sequence (e), and ADC imaging (f) when the symptoms subsided revealed improvement in the dural enhancement (arrowheads in [d] and [e]) and gyral swelling with normal ADC signal. Features are in keeping with SMART syndrome. Interval reduction in pachymeningeal enhancement and dilatation of the ventricles suggested improvement of overshunting. Incidental finding of an extra axial cystic lesion at the pineal region was suggestive of an arachnoid cyst (curved arrows in [b] and [e]) which remained stable in size for >5 years.

as opposed to the unilaterality and predominant cortical involvement of SMART syndrome, which usually aids in radiological differentiation from PRES.

## RADIATION-INDUCED NEOPLASM

Radiation-induced tumour is generally defined as a secondary neoplasm of different histology, developing in the radiation field after an asymptomatic latency period. Meningioma is the most common radiation-induced central nervous system tumour and World Health Organization grade I meningioma is the most common subtype (Figure 14).[16] The overall survival is comparable to that of de novo meningiomas with similar grades.[17]

### Acute to Subacute Radiation-Induced Injury

Acute radiation encephalopathy can occur in days to weeks after irradiation, due to alterations in capillary permeability, disruption of the blood-brain barrier, and development of vasogenic oedema. Clinical manifestations may include acute neurological symptoms such as nausea, vomiting, drowsiness, headache, or acute worsening of pre-existing neurological symptoms.[11] Diffuse brain swelling, T2-weighted hyperintensity in the white matter, or new or enlarged contrast-enhancing lesions in the vicinity of irradiation can be demonstrated on MRI. Corticosteroids may be helpful to control patients' signs and symptoms.[11]

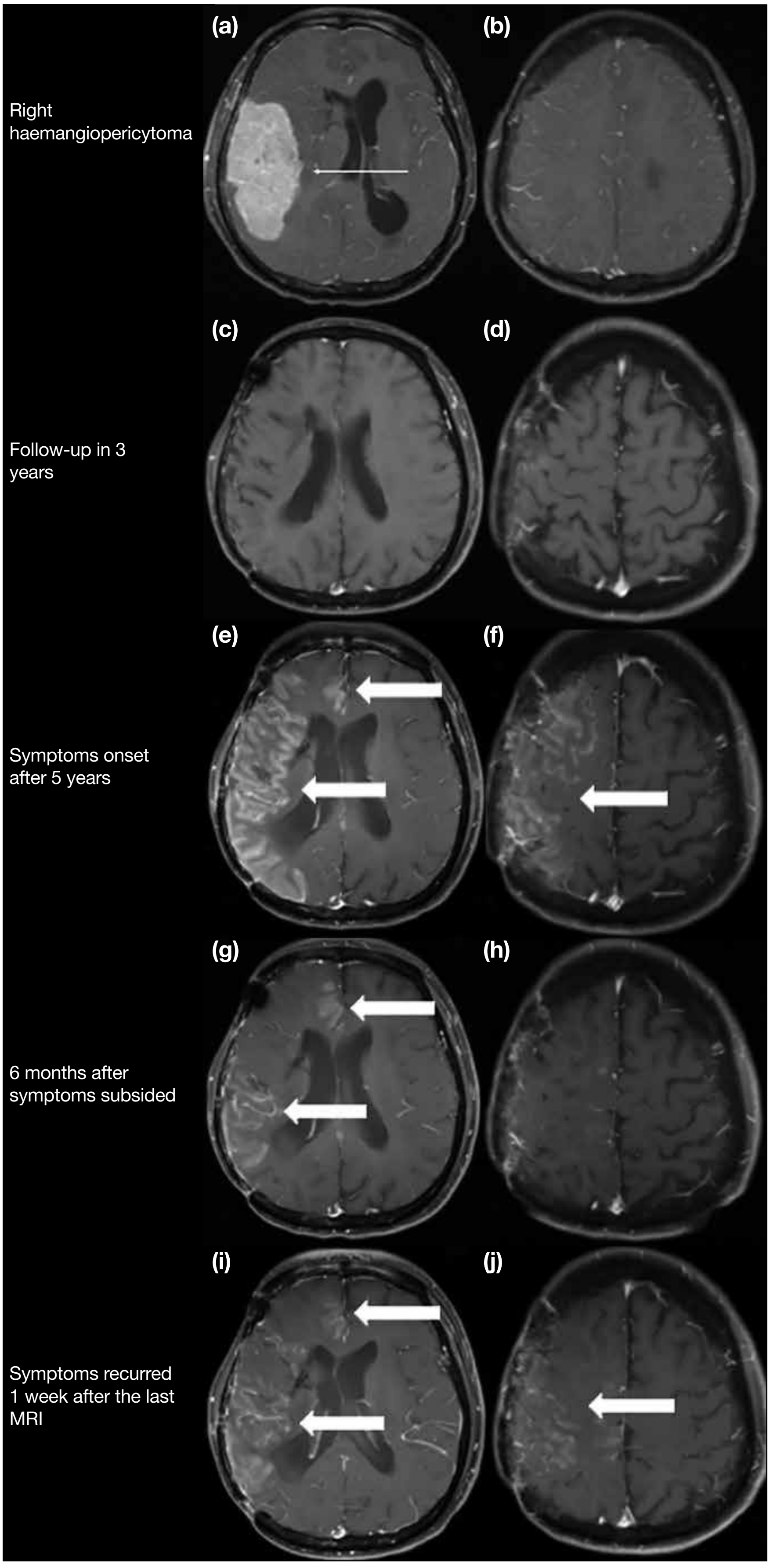


**Figure 13.** Stroke-like migraine attacks after radiation therapy (SMART) syndrome. (a, c, e, g, and i) show post-contrast T1-weighted fat suppression (FS) sequence at the level of lateral ventricles over time and (b, d, f, h, and j) show post-contrast T1-weighted FS sequence acquired above the ventricles. A 40-year-old patient presented with an extra-axial right supratentorial contrast-enhancing mass (thin arrow in [a]), which was proven to be a haemangiopericytoma, was treated with total excision (a and b) followed by adjuvant radiotherapy. No disease recurrence was identified in follow-up magnetic resonance imaging (MRI) performed 3 years after the excision (c and d). The patient presented again with intermittent and reversible left-hand weakness and numbness and seizures 5 years after the operation. MRI (e and f) demonstrated gyriform and leptomeningeal enhancement involving the right cerebral hemisphere (arrows). Follow-up MRI performed 6 months later when symptoms subsided (g and h) illustrated radiological improvement of the contrast enhancement (arrows in [g]). However, symptoms recurred shortly after the MRI and rescan in 1 week showed new leptomeningeal enhancement at the high right frontoparietal lobe (arrows in [i] and [j]). Overall features are most compatible with recurrent SMART syndrome.

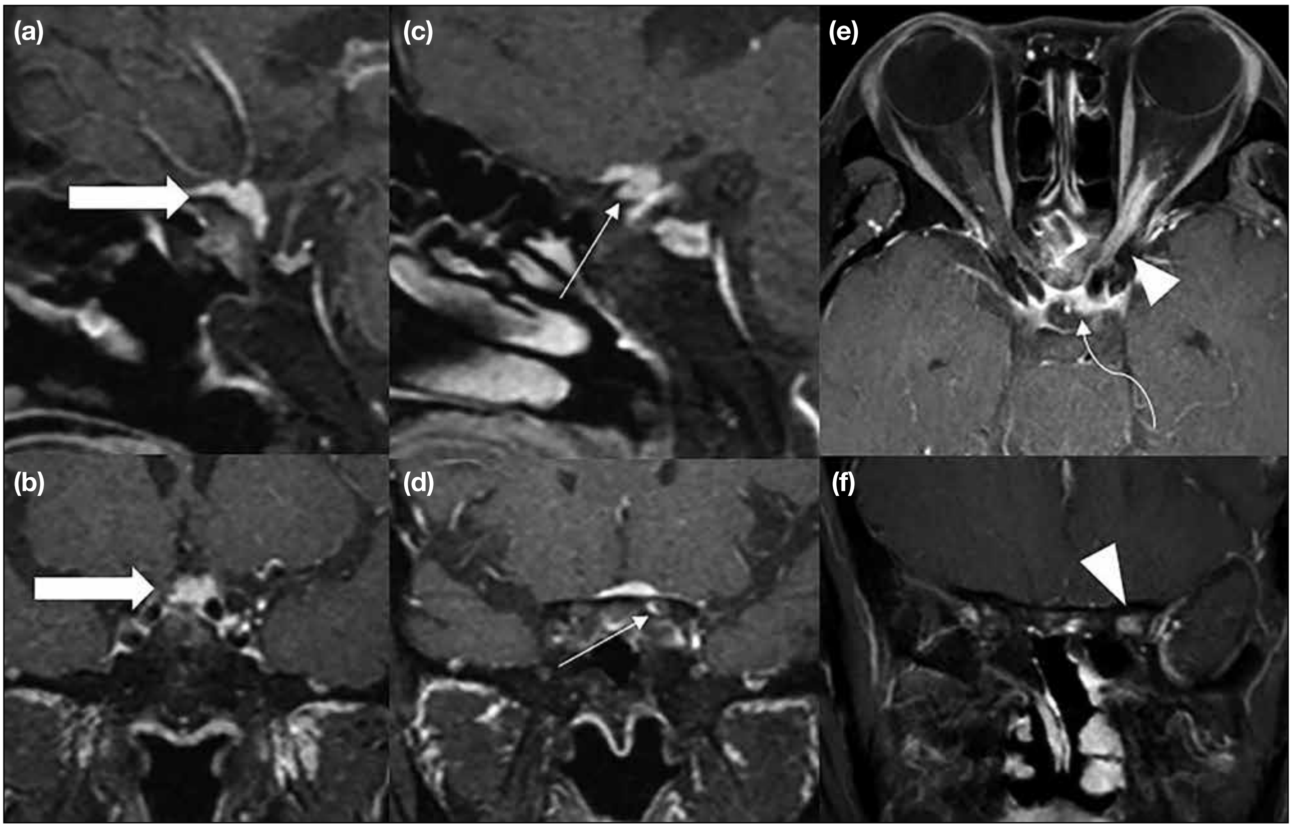


**Figure 14.** Radiation-induced meningioma in a 62-year-old patient. (a and c) and (b and d) show sagittal and coronal post-contrast T1-weighted fat saturation sequences performed 10 years after excision and radiotherapy of left pituitary microadenoma, respectively. (e) and (f) show axial and coronal post-contrast T1-weighted fat saturation sequences of magnetic resonance imaging (MRI) performed 15 years after radiotherapy, respectively. MRI performed 10 years after treatment revealed the dural tail and suprasellar location of an extra-axial enhancing lesion at the planum sphenoidale (arrows in [a] and [b]) with early extension to the intracanalicular segment of the left optic nerve sheath (thin arrows in [c] and [d]). Partial excision was performed, revealing World Health Organization grade I meningioma. Follow-up MRI performed 15 years after the initial treatment demonstrated 'tram-track' enhancement of the left optic nerve sheath (arrowheads in [e] and [f]) with a sharp anterior margin at the intraorbital segment. Residual tumour in the left suprasellar region encased the left internal carotid artery (curved arrow in [e]). Overall features are compatible with radiation-induced meningioma with progressive left optic nerve sheath involvement.

## RADIATION-INDUCED LEUCOENCEPHALOPATHY

Radiation-induced leucoencephalopathy generally refers to delayed radiation-induced white matter injury with a reported incidence of up to 34% in patients receiving lower radiation dosages, e.g., in whole-brain radiotherapy. The mechanisms of this leucoencephalopathy include damage to the oligodendrocytes, resulting in axonal demyelination, disruption of vascular endothelium, and focal mineralisation.[11] Patients may be asymptomatic or present with varying degrees of neurocognitive decline. Imaging features typically include progressive symmetric and confluent T2/FLAIR hyperintense signals mainly in the periventricular white matter and brain atrophy (Figure 15).[6]

## CONCLUSION

The combination of conventional and advanced MRI techniques in post-treatment brain tumour imaging aids radiologists in distinguishing between treatment response and treatment-related changes and recognising post-treatment complications. Familiarity with these techniques might help to avoid unnecessary alteration of the patients' management or invasive procedures.

## REFERENCES

1. Leao DJ, Craig PG, Godoy LF, Leite CC, Policeni B. Response assessment in neuro-oncology criteria for gliomas: practical approach using conventional and advanced techniques. AJNR Am J Neuroradiol. 2020;41:10-20.
2. Stupp R, Mason WP, van den Bent MJ, Weller M, Fisher B, Taphoorn MJ, et al. Radiotherapy plus concomitant and adjuvant temozolomide for glioblastoma. N Engl J Med. 2005;352:987-96.

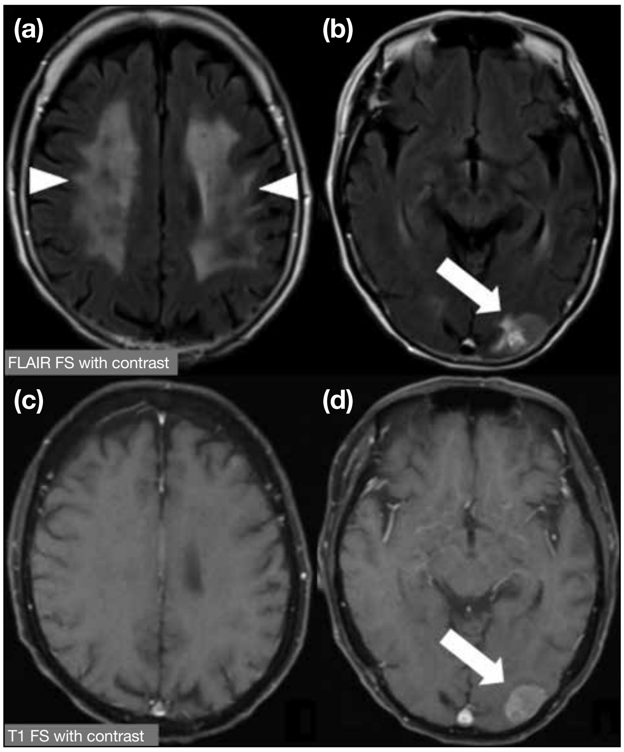


**Figure 15.** Radiation-induced leucoencephalopathy. A 70-year-old patient with metastatic pulmonary malignancy was diagnosed with brain metastases and managed with whole-brain radiotherapy (WBRT). Follow-up magnetic resonance post-contrast fluid-attenuation inversion recovery (FLAIR) fat suppression (FS) sequences (a and b) and post-contrast T1-weighted FS sequences (c and d) performed 4 years after WBRT demonstrated bilateral non-enhancing FLAIR hyperintensity involving the supratentorial white matter (arrowheads in [a]). Features could represent radiotherapy-induced leucoencephalopathy. A contrast-enhancing lesion is illustrated in the left occipital lobe (arrows in [b] and [d]), suggestive of brain metastasis.

3. Stupp R, Taillibert S, Kanner A, Read W, Steinberg D, Lhermitte B, et al. Effect of tumor-treating fields plus maintenance temozolomide vs maintenance temozolomide alone on survival in patients with glioblastoma: a randomized clinical trial. JAMA. 2017;318:2306-16.
4. Wen PY, Macdonald DR, Reardon DA, Cloughesy TF, Sorensen AG, Galanis E, et al. Updated response assessment criteria for high-grade gliomas: response assessment in Neuro-Oncology Working Group. J Clin Oncol. 2010;28:1963-72.
5. Prager AJ, Maritnez N, Beal K, Omuro A, Zhang Z, Young RJ. Diffusion and perfusion MRI to differentiate treatment-related changes including pseudoprogression from recurrent tumors in high-grade gliomas with histopathologic evidence. AJNR Am J Neuroradiol. 2015;36:877-85.
6. Kessler AT, Bhatt AA. Brain tumour post-treatment imaging and treatment-related complications. Insights Imaging. 2018;9:1057-75.
7. Jackson A, Jayson GC, Li KL, Zhu XP, Checkley DR, Tessier JJ, et al. Reproducibility of quantitative dynamic contrast-enhanced MRI in newly presenting glioma. Br J Radiol. 2003;76:153-62.
8. Heye AK, Culling RD, Valdés Hernández MdC, Thrippleton MJ, Wardlaw JM. Assessment of blood-brain barrier disruption using dynamic contrast-enhanced MRI. A systematic review. Neuroimage Clin. 2014;6:262-74.
9. Narang J, Jain R, Arbab AS, Mikkelsen T, Scarpace L, Rosenblum ML, et al. Differentiating treatment-induced necrosis from recurrent/progressive brain tumor using non-model–based semiquantitative indices derived from dynamic contrast-enhanced T1-weighted MR perfusion. Neuro Oncol. 2011;13:1037-46.
10. Chung WJ, Kim HS, Kim N, Choi CG, Kim SJ. Recurrent glioblastoma: optimum area under the curve method derived from dynamic contrast-enhanced T1-weighted perfusion MR imaging. Radiology. 2013;269:561-8.
11. Katsura M, Sato J, Akahane M, Furuta T, Mori H, Abe O. Recognizing radiation-induced changes in the central nervous system: where to look and what to look for. Radiographics. 2021;41:224-48.
12. Kumar AJ, Leeds NE, Fuller GN, Van Tassel P, Maor MH, Sawaya RE, et al. Malignant gliomas: MR imaging spectrum of radiation therapy- and chemotherapy-induced necrosis of the brain after treatment. Radiology. 2000;217:377-84.
13. Black DF, Morris JM, Lindell EP, Krecke KN, Worrell GA, Barleson JD, et al. Stroke-like migraine attacks after radiation therapy (SMART) syndrome is not always completely reversible: a case series. AJNR Am J Neuroradiol. 2013;34:2298-303.
14. Patel UK, Patel K, Malik P, Elkady A, Patel Nidhi, Lunagariya A. Stroke-like migraine attacks after radiation therapy (SMART) syndrome—a case series and review. Neurol Sci. 2020;41:3123-34.
15. Fugate JE, Rabinstein AA. Posterior reversible encephalopathy syndrome: clinical and radiological manifestations, pathophysiology, and outstanding questions. Lancet Neurol. 2015;14:914-25.
16. Yamanaka R, Hayano A, Kanayama T. Radiation-induced meningiomas: an exhaustive review of the literature. World Neurosurg. 2017;97:635-44.e8.
17. Lee JW, Wernicke AG. Risk and survival outcomes of radiation-induced CNS tumors. J Neurooncol. 2016;129:15-22.